

Nematic-order state characteristic energy and its connection to enhancement of superconductivity in cuprate superconductors

Zhangkai Cao¹, Xingyu Ma¹, Yiqun Liu², Huaiming Guo³, and Shiping Feng^{1*}

¹*Department of Physics, Beijing Normal University, Beijing 100875, China*

²*School of Physics, Nanjing University, Nanjing 210093, China and*

³*School of Physics, Beihang University, Beijing 100191, China*

The new development in sublattice-phase-resolved imaging of electronic structure now allow for the visualisation of the nematic-order state characteristic energy of cuprate superconductors in a wide doping regime. However, it is still unclear how this nematic-order state characteristic energy is correlated with the enhancement of superconductivity. Here the doping dependence of the nematic-order state characteristic energy in cuprate superconductors and of its possible connection to the enhancement of superconductivity is investigated within the framework of the kinetic-energy-driven superconductivity. It is shown that the magnitude of the nematic-order state characteristic energy is found to be particularly large in the underdoped regime, then it smoothly decreases upon the increase of doping, in full agreement with the corresponding experimental observations. Moreover, the theory also shows that the nematic-order state strength dependence of the characteristic energy coincides with the corresponding nematic-order state strength dependence of the enhancement of superconductivity, suggesting a possible connection between the nematic-order state characteristic energy and the enhancement of the superconductivity.

PACS numbers: 74.25.Jb, 74.25.Dw, 74.20.Mn, 74.72.-h

In cuprate superconductors¹, the strongly correlated motion of the electrons is confined to the square-lattice CuO₂ planes^{2,3}. However, this strong electron correlation also induces the system to exhibit numerous ordering tendencies⁴⁻⁹. In addition to superconductivity, a variety of spontaneous symmetry-breaking orders have been observed experimentally, indicating the coexistence and intertwinement between these spontaneous symmetry-breaking orders and superconductivity⁴⁻⁹. Among these spontaneous symmetry-breaking orders, the most distinct form of order is electronically nematic order⁶⁻⁹, which corresponds to that the electronic structure preserves the translation symmetry but breaks the rotation symmetry of the underlying square-lattice CuO₂ plane. As a natural consequence of a doped Mott insulator, the manipulation of the particular characteristics of the superconducting (SC) state with coexisting electronic nematicity through the control of doping and strength of the electronic nematicity is hotly debated and has been believed to be key to the understanding of the problem of why cuprate superconductors exhibit a number of the anomalous properties⁴⁻⁹.

Experimentally, scanning tunneling spectroscopy (STS) is a direct tool in the exploration of the quasiparticle scattering interference (QSI) of cuprate superconductors¹⁰⁻¹². Moreover, this QSI has been used to elucidate the nature of the quasiparticle excitation and of its interplay with spontaneous symmetry-breaking orders and superconductivity¹⁰⁻¹². In the early STS measurements, some characteristic features of the nematic-order state quasiparticle excitation have been well-established¹³⁻²³, however, the evolution of the nematic-order state characteristic energy with doping in the entire range of the SC dome remains puzzling. In recent years, the instrumentation for sublattice-phase-resolved

imaging of electronic structure has improved dramatically, allowing this experimental technique to visualize simultaneously the doping and energy dependence of QSI in the SC-state with coexisting symmetry-breaking ordered states^{12,24}. In this case, as a compensation for the early experimental studies²¹⁻²³, this experimental technique have purported to measure the nematic-order state tunneling conductance of Bi₂Sr₂CaCu₂O_{8+δ} over a large field of view, perform a Fourier transform (FT), and analyze data from distinct regions of momentum space²⁴. In particular, with a careful examination of these high-resolution of the STS data, the evolution of the nematic-order state characteristic energy with doping is identified, where measured on the samples whose doping spans the pseudogap regime, the nematic-state characteristic energy and pseudogap energy are, within the experimental error, identical²⁴. Moreover, the very importance is that these experimental data have identified the electronically nematic order exists across the entire range of the SC dome. On the basis of these experimental results, it thus has been argued that the pseudogap is a consequence of a tendency towards an electronically ordered state that is a coexistence of the nematic order and charge orders and breaks both the translation and rotation symmetry^{9,24}.

Although the doping dependence of the nematic-order state characteristic energy in cuprate superconductors has been well-identified experimentally in the entire range of the SC dome²⁴, its full understanding is still a challenging issue. In particular, it is still unclear how this nematic-order state characteristic energy evolves with the strength of the electronic nematicity. In our recent study²⁵, the intertwinement of the electronic nematicity with superconductivity in cuprate superconductors has been studied based on the kinetic-energy-driven superconductivity, where we have shown that the electronic

nematicity enhances superconductivity. Moreover, we²⁵ have also shown that the order parameter of the electronic nematicity achieves its maximum in the nematic-order state characteristic energy, and then decreases rapidly as the energy moves away from the nematic-order state characteristic energy, in agreement with the experimental observation²⁴. However, a natural question is whether the nematic-state characteristic energy is correlated with the enhancement of superconductivity or not? In this paper, as a complement of our recent analysis of the exotic features of the quasiparticle excitation in the SC-state with coexisting electronic nematicity²⁵, we study the doping dependence of the nematic-order state characteristic energy and of its possible connection to the enhancement of superconductivity, where one of our main results is that in a striking similar to the doping dependence of the pseudogap state, the nematic-order state is particularly obvious in the underdoped regime, i.e., the magnitude of the nematic-order state characteristic energy is particularly large in the underdoped regime, and then it monotonically decreases with the increase of doping, in full agreement with the corresponding experimental observations²⁴. More specifically, our results also show both the nematic-order state characteristic energy and enhancement of the SC transition temperature T_c exhibit the same nematic-order state strength dependence, i.e., the maximal nematic-order state characteristic energy (then the maximal T_c) occurs at around the optimal strength of the electronic nematicity, and then decreases in both weak and strong strength regions, indicating a possible connection between the nematic-order state characteristic energy and the enhancement of superconductivity.

When the quasiparticle scattering mixes the states \mathbf{k} and $\mathbf{k} + \mathbf{q}$, a QSI pattern with the wave vector \mathbf{q} appears in the norm of the quasiparticle wave function and the local density of states modulations with the wave length $\lambda = 2\pi/|\mathbf{q}|$ appear, reflecting a basic fact that the QSI pattern manifests itself is an autocorrelation between the quasiparticle bands $E_{\mathbf{k}}$ and $E_{\mathbf{k}+\mathbf{q}}$ ^{11,12}. In other words, the intensity in the QSI pattern is proportional to the spectral intensities of the single-particle excitation spectra at the momenta \mathbf{k} and $\mathbf{k} + \mathbf{q}$, while the sharp intensity peaks in the QSI pattern then are corresponding to the highest joint density of states. This is why the quasiparticle scattering processes, the quasiparticle momentum-space structure, and the dispersion of the peaks in the QSI pattern as a function of energy are interpreted in terms of the octet scattering model^{26,27}, and yields the crucial information of the quasiparticle excitation. More importantly, by the analysis of the typical feature of the Bragg peaks in a QSI pattern, one is considering the phenomena that occur with the periodicity of the underlying square lattice and which qualify any rotation symmetry-breaking^{10-12,21-24}. Likewise, the autocorrelation between the quasiparticle bands $E_{\mathbf{k}}$ and $E_{\mathbf{k}+\mathbf{q}}$ can be also measured in terms of the angle-resolved photo-

mission spectroscopy (ARPES) autocorrelation²⁸,

$$\bar{C}_{\varsigma}(\mathbf{q}, \omega) = \frac{1}{N} \sum_{\mathbf{k}} I_{\varsigma}(\mathbf{k} + \mathbf{q}, \omega) I_{\varsigma}(\mathbf{k}, \omega), \quad (1)$$

where N is the number of lattice sites, and $I_{\varsigma}(\mathbf{k}, \omega)$ is the single-particle excitation spectrum, while the summation of momentum \mathbf{k} is extended up to the second Brillouin zone (BZ)²⁸ for the discussion of QSI together with the Bragg scattering. This ARPES autocorrelation in Eq. (1) describes the correlation of the spectral intensities of the single-particle excitation spectra at two different momenta \mathbf{k} and $\mathbf{k} + \mathbf{q}$, separated by a momentum transfer \mathbf{q} , at a fixed energy, and is effectively the momentum-resolved joint density of states. In particular, it has been demonstrated experimentally^{28,29} that the peaks, the momentum-space structure, and the dispersion of the peaks in the ARPES autocorrelation pattern are directly related to the peaks, the momentum-space structure, and the dispersion of the peaks in the QSI pattern^{10-12,21-24}, respectively, and can be also explained straightforwardly in terms of the octet scattering model. This is why the characteristic features of QSI can be also obtained in terms of the ARPES autocorrelation.

The single-particle excitation spectrum $I_{\varsigma}(\mathbf{k}, \omega)$ in Eq. (1) is proportional to the electron spectral function $A_{\varsigma}(\mathbf{k}, \omega)$ as,

$$I_{\varsigma}(\mathbf{k}, \omega) \propto n_F(\omega) A_{\varsigma}(\mathbf{k}, \omega), \quad (2)$$

where $n_F(\omega)$ is the fermion distribution, while the electron spectral function $A_{\varsigma}(\mathbf{k}, \omega)$ in the SC-state with coexisting electronic nematicity can be obtained directly from the full electron diagonal propagator as $A_{\varsigma}(\mathbf{k}, \omega) = -2\text{Im}G_{\varsigma}(\mathbf{k}, \omega)$.

Now our goal is to evaluate this full electron diagonal propagator $G_{\varsigma}(\mathbf{k}, \omega)$ starting from a microscopic SC theory. The strongly correlated motion of the electrons in cuprate superconductors is restricted to the square-lattice CuO₂ planes^{2,3} as mentioned above, and then the unconventional properties come from the strongly correlated motion of the electrons in these CuO₂ planes. In particular, as originally emphasized by Anderson³⁰, the essential physics of the strongly correlated motion of the electrons in a square-lattice CuO₂ plane can be described properly by the t - J model,

$$H = - \sum_{l\hat{\eta}\sigma} t_{\hat{\eta}} C_{l\sigma}^{\dagger} C_{l+\hat{\eta}\sigma} + \sum_{l\hat{\tau}\sigma} t'_{\hat{\tau}} C_{l\sigma}^{\dagger} C_{l+\hat{\tau}\sigma} + \mu \sum_{l\sigma} C_{l\sigma}^{\dagger} C_{l\sigma} + \sum_{l\hat{\eta}} J_{\hat{\eta}} \mathbf{S}_l \cdot \mathbf{S}_{l+\hat{\eta}}, \quad (3)$$

where $\hat{\eta} = \pm\hat{x}, \pm\hat{y}$ represents the nearest neighbor (NN) sites of a given site l , $\hat{\tau} = \pm\hat{x} \pm \hat{y}$ represents the next NN sites of a given site l , $C_{l\sigma}^{\dagger}$ and $C_{l\sigma}$ are the electron creation and annihilation operators, respectively, \mathbf{S}_l is the spin operator with its components S_l^x , S_l^y , and S_l^z , while μ is the chemical potential. For the discussions of

the exotic features of the SC-state with coexisting electronic nematicity, the next NN hoping amplitude in the t - J model (3) is chosen as $t'_\hat{x} = t'$, while the NN hoping amplitude $t_{\hat{y}}$ has the following form¹³,

$$t_{\hat{x}} = (1 - \varsigma)t, \quad t_{\hat{y}} = (1 + \varsigma)t, \quad (4)$$

which is strongly anisotropic along the \hat{x} and \hat{y} directions and follows from the previous analyses of the exotic features in the nematic-order state³¹⁻³⁴. In particular, the anisotropic NN hoping amplitude in Eq. (4) has been experimentally verified¹³ in terms of the standard tight-binding model to fit the nematic-order state ARPES spectrum¹³. Concomitantly, this anisotropic NN hoping amplitude in Eq. (4) induces the anisotropic NN exchange coupling $J_{\hat{x}} = (1 - \varsigma)^2 J$ and $J_{\hat{y}} = (1 + \varsigma)^2 J$ in the t - J model (3). Moreover, the magnitude of the anisotropic parameter ς in Eq. (4) has been considered to represent the strength of the electronic nematicity in the system¹³, and in this sense, the anisotropic NN hoping amplitudes in Eq. (4) also indicate that the rotation symmetry is broken already in the starting t - J model (3). In cuprate superconductors, although the values of J , t , and t' are believed to vary somewhat from compound to compound, the commonly used parameters in this paper are chosen as $t/J = 3$, $t'/t = 1/3$, and $J = 100$ meV as in our previous discussions²⁵.

Within the t - J model (3), the kinetic-energy-driven superconductivity developed in the case of the absence of the electronic nematicity³⁵⁻³⁸ has been generalized very recently to discuss the intertwinement of the electronic nematicity with superconductivity in cuprate superconductors²⁵, where the breaking of the rotation symmetry due to the presence of the electronic nematicity is verified by the inequivalence on the average of the electronic structure at the two Bragg scattering sites. Following up on this recent work on the intertwinement of the electronic nematicity with superconductivity²⁵, the full electron diagonal propagator of the t - J model (3) can be expressed explicitly as,

$$G_\varsigma(\mathbf{k}, \omega) = \frac{1}{\omega - \varepsilon_{\mathbf{k}}^{(\varsigma)} - \Sigma_{\text{tot}}^{(\varsigma)}(\mathbf{k}, \omega)}, \quad (5)$$

where the orthorhombic energy dispersion in the tight-binding approximation is obtained directly from the t - J model (3) as,

$$\varepsilon_{\mathbf{k}}^{(\varsigma)} = -4t[(1 - \varsigma)\gamma_{\mathbf{k}_x} + (1 + \varsigma)\gamma_{\mathbf{k}_y}] + 4t'\gamma'_{\mathbf{k}} + \mu, \quad (6)$$

with $\gamma_{\mathbf{k}_x} = \cos k_x/2$, $\gamma_{\mathbf{k}_y} = \cos k_y/2$, $\gamma'_{\mathbf{k}} = \cos k_x \cos k_y$, while the total self-energy is a specific combination of the normal self-energy $\Sigma_{\text{ph}}^{(\varsigma)}(\mathbf{k}, \omega)$ in the particle-hole channel and the anomalous self-energy $\Sigma_{\text{pp}}^{(\varsigma)}(\mathbf{k}, \omega)$ in the particle-particle channel as,

$$\Sigma_{\text{tot}}^{(\varsigma)}(\mathbf{k}, \omega) = \Sigma_{\text{ph}}^{(\varsigma)}(\mathbf{k}, \omega) + \frac{|\Sigma_{\text{pp}}^{(\varsigma)}(\mathbf{k}, \omega)|^2}{\omega + \varepsilon_{\mathbf{k}}^{(\varsigma)} + \Sigma_{\text{ph}}^{(\varsigma)}(\mathbf{k}, -\omega)}, \quad (7)$$

with the normal self-energy $\Sigma_{\text{ph}}^{(\varsigma)}(\mathbf{k}, \omega)$ and anomalous self-energy $\Sigma_{\text{pp}}^{(\varsigma)}(\mathbf{k}, \omega)$ that have been given explicitly in Ref. 25, where the sharp peak visible for temperature $T \rightarrow 0$ in the normal (anomalous) self-energy is actually a δ -function, broadened by a small damping used in the numerical calculation at a finite lattice. The calculation in this paper for the normal (anomalous) self-energy is performed numerically on a 120×120 lattice in momentum space, with the infinitesimal $i0_+ \rightarrow i\Gamma$ replaced by a small damping $\Gamma = 0.05J$.

With the above full electron diagonal Green's function (5), the electron spectral function $A_\varsigma(\mathbf{k}, \omega)$ in the SC-state with coexisting electronic nematicity now can be obtained explicitly as,

$$A_\varsigma(\mathbf{k}, \omega) = \frac{-2\text{Im}\Sigma_{\text{tot}}^{(\varsigma)}(\mathbf{k}, \omega)}{[\omega - \varepsilon_{\mathbf{k}}^{(\varsigma)} - \text{Re}\Sigma_{\text{tot}}^{(\varsigma)}(\mathbf{k}, \omega)]^2 + [\text{Im}\Sigma_{\text{tot}}^{(\varsigma)}(\mathbf{k}, \omega)]^2}, \quad (8)$$

where $\text{Re}\Sigma_{\text{tot}}^{(\varsigma)}(\mathbf{k}, \omega)$ and $\text{Im}\Sigma_{\text{tot}}^{(\varsigma)}(\mathbf{k}, \omega)$ are the real and imaginary parts of the total self-energy $\Sigma_{\text{tot}}(\mathbf{k}, \omega)$, respectively. Substituting this electron spectral function $A_\varsigma(\mathbf{k}, \omega)$ in Eq. (8) into Eqs. (2) and (1), we therefore obtain the ARPES autocorrelation $\bar{C}_\varsigma(\mathbf{q}, \omega)$ within the framework of the kinetic-energy-driven superconductivity.

In the presence of the electronic nematicity, the original electronic structure with the four-fold (C_4) rotation symmetry on the square lattice in the absence of the electronic nematicity is broken up into that with a residual two-fold (C_2) rotation symmetry, while such an aspect should be reflected in QSI. For a convenience in the following discussions, the ARPES autocorrelation $\bar{C}_\varsigma(\mathbf{q}, \omega)$ pattern²⁵ in momentum-space for the binding-energy $\omega = 94$ meV at doping $\delta = 0.06$ with temperature $T = 0.002J$ and the strength of the electronic nematicity $\varsigma = 0.006$ is replotted in Fig. 1a, where the locations of the Bragg peaks $\mathbf{Q}_x^{(B)} = [\pm 2\pi, 0]$ along the \hat{x} axis and $\mathbf{Q}_y^{(B)} = [0, \pm 2\pi]$ along the \hat{y} axis are indicated by the circles, while $\mathbf{q}_1, \mathbf{q}_2, \mathbf{q}_3, \mathbf{q}_4, \mathbf{q}_5, \mathbf{q}_6$, and \mathbf{q}_7 are different quasiparticle scattering wave vectors. For a better comparison, the corresponding experimental result²⁴ of the QSI pattern observed from $\text{Bi}_2\text{Sr}_2\text{CaCu}_2\text{O}_{8+\delta}$ for the bind-energy $\omega = 94$ meV at doping $\delta = 0.06$ is also shown in Fig. 1b. Apparently, the momentum-space structure of the ARPES autocorrelation pattern in the SC-state with coexisting electronic nematicity obtained from Eq. (1) is qualitative consistent with the corresponding momentum-space structure of the QSI pattern detected experimentally from $\text{Bi}_2\text{Sr}_2\text{CaCu}_2\text{O}_{8+\delta}$, where the characteristic features of two distinct classes of the broken-symmetry states have been summarized as²⁵: (i) For the quasiparticle scattering processes with the corresponding scattering wave vectors $\mathbf{q}_1, \mathbf{q}_4$, and \mathbf{q}_5 , the amplitudes of the quasiparticle scattering wave vectors are respectively inequivalent to their symmetry-corresponding partners, while for the quasiparticle scattering process with the corresponding quasiparticle scattering wave vectors $\mathbf{q}_2, \mathbf{q}_3, \mathbf{q}_6$, and \mathbf{q}_7 , the scattering wave vectors and

their symmetry-equivalent partners occur with equal amplitudes, indicating that the peaks at the corresponding scattering wave vectors \mathbf{q}_1 , \mathbf{q}_4 , and \mathbf{q}_5 are the signatures of the electronically ordered states with broken both rotation and translation symmetries, while the peaks with the corresponding scattering wave vectors \mathbf{q}_2 , \mathbf{q}_3 , \mathbf{q}_6 , and \mathbf{q}_7 are the signatures of the electronically ordered states with broken translation symmetry only; (ii) The intensity of the peak at the Bragg wave vector $\mathbf{Q}_x^{(B)}$ is different from that at the Bragg wave vector $\mathbf{Q}_y^{(B)}$. This difference leads to the inequivalence on the average of the electronic structure at the two Bragg scattering sites $\mathbf{Q}_x^{(B)}$ and $\mathbf{Q}_y^{(B)}$, and therefore shows that the Bragg peaks at the wave vectors $\mathbf{Q}_x^{(B)}$ and $\mathbf{Q}_y^{(B)}$ are the signature of the nematic-order state with the broken C_4 rotation symmetry.

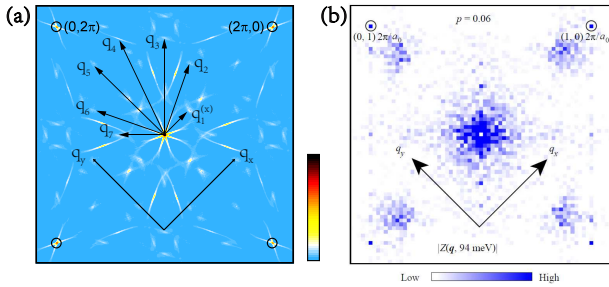


FIG. 1: (Color online) (a) The ARPES autocorrelation pattern in momentum-space for the binding-energy $\omega = 94$ meV at doping $\delta = 0.06$ with temperature $T = 0.002J$ and the strength of the electronic nematicity $\xi = 0.006$. (b) The corresponding experimental result of the quasiparticle scattering interference pattern of $\text{Bi}_2\text{Sr}_2\text{CaCu}_2\text{O}_{8+\delta}$ for the binding-energy $\omega = 94$ meV at doping $\delta = 0.06$ taken from Ref. 24.

We are now ready to discuss the doping dependence of the nematic-order state characteristic energy and of its possible connection to the enhancement of superconductivity. In our previous studies²⁵, the order parameter of the electronic nematicity has been given as,

$$N^{(\bar{C}_\xi)}(\omega) = \frac{\bar{C}_\xi^{(x)}(\omega) - \bar{C}_\xi^{(y)}(\omega)}{\bar{C}_\xi^{(x)}(\omega) + \bar{C}_\xi^{(y)}(\omega)}, \quad (9)$$

where $\bar{C}_\xi^{(x)}(\omega) = (1/N) \sum_{\mathbf{q} \in \{\mathbf{Q}_x^{(B)}\}} \bar{C}_\xi(\mathbf{q}, \omega)$ and $\bar{C}_\xi^{(y)}(\omega) = (1/N) \sum_{\mathbf{q} \in \{\mathbf{Q}_y^{(B)}\}} \bar{C}_\xi(\mathbf{q}, \omega)$, with the summation $\mathbf{q} \in \{\mathbf{Q}_x^{(B)}\}$ [$\mathbf{q} \in \{\mathbf{Q}_y^{(B)}\}$] that is restricted to the extremely small area $\{\mathbf{Q}_x^{(B)}\}$ [$\{\mathbf{Q}_y^{(B)}\}$] at around $\mathbf{Q}_x^{(B)}$ [$\mathbf{Q}_y^{(B)}$]. This definition in Eq. (9) is confronted with the reduction of the size effect in a finite-lattice calculation. This follows a basic fact that the calculation for the normal and anomalous self-energies in Eq. (7) is performed numerically on a 120×120 lattice in momentum space as we have mentioned above, with the infinitesimal $i0_+ \rightarrow i\Gamma$ replaced by a small damping $\Gamma = 0.05J$,

which leads to that the peak weight of the ARPES autocorrelation $\bar{C}_\xi(\mathbf{q}, \omega)$ in Eq. (1) at the Bragg wave vector $\mathbf{Q}_x^{(B)}$ [$\mathbf{Q}_y^{(B)}$] spreads on the extremely small area $\{\mathbf{Q}_x^{(B)}\}$ [$\{\mathbf{Q}_y^{(B)}\}$] at around the $\mathbf{Q}_x^{(B)}$ [$\mathbf{Q}_y^{(B)}$] point. The summation of these spread weights in $\bar{C}_\xi^{(x)}(\omega)$ and $\bar{C}_\xi^{(y)}(\omega)$ at around this extremely small area $\{\mathbf{Q}_x^{(B)}\}$ [$\{\mathbf{Q}_y^{(B)}\}$] can reduce the size effect in the finite-lattice calculation. If this order parameter $N^{(\bar{C}_\xi)}(\omega)$ is non-zero, the break of the C_4 rotation symmetry is occurring. In Fig. 2a, we plot the nematic-order state order parameter $N^{(\bar{C}_\xi)}(\omega)$ as a function of binding-energy at $\delta = 0.06$ with $T = 0.002J$ for the strength of the electronic nematicity $\xi = 0.006$. For a direct comparison, the corresponding experimental result²⁴ of the energy dependence of the nematic-order state order parameter observed from $\text{Bi}_2\text{Sr}_2\text{CaCu}_2\text{O}_{8+\delta}$ at doping $\delta = 0.06$ is also shown in Fig. 2b. It thus shows clearly that the experimental result²⁴ of the energy dependence of the nematic-order state order parameter is well reproduced, where $N^{(\bar{C}_\xi)}(\omega)$ reaches its maximum in the characteristic energy ω_{\max} , however, when the energy is turned away from this characteristic energy ω_{\max} , $N^{(\bar{C}_\xi)}(\omega)$ drops rapidly. Moreover, this anticipated characteristic energy $\omega_{\max} \sim 0.936J = 93.6$ meV is well consistent with the experimental result²⁴ of $E_{\max}^{(N)} \sim 94$ meV observed on $\text{Bi}_2\text{Sr}_2\text{CaCu}_2\text{O}_{8+\delta}$ at doping $\delta = 0.06$. This energy dependence of $N^{(\bar{C}_\xi)}(\omega)$ with non-zero values therefore further verifies the nematic-order state with broken C_4 rotation symmetry in a wide energy range.

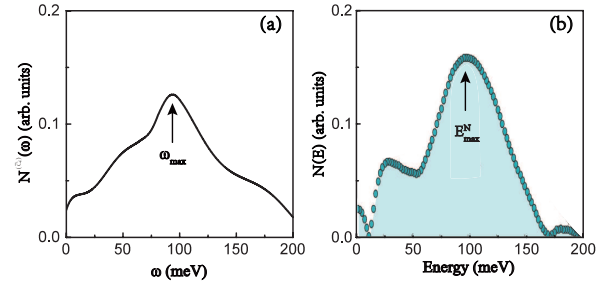


FIG. 2: (Color online) (a) The order parameter of the nematic-order state as a function of energy at $\delta = 0.06$ with $T = 0.002J$ for the strength of the electronic nematicity $\xi = 0.006$, where the arrow indicates the position of the peak at the characteristic energy. (b) The corresponding experimental result observed from $\text{Bi}_2\text{Sr}_2\text{CaCu}_2\text{O}_{8+\delta}$ at doping $\delta = 0.06$ taken from Ref. 24.

As a natural consequence of the doped Mott insulators, the nematic-order state characteristic energy ω_{\max} also evolve strongly with doping. For a better understanding of the doping dependence of ω_{\max} , we plot the result of ω_{\max} as a function of doping with $T = 0.002J$ for the strength of the electronic nematicity $\xi = 0.006$ in Fig. 3a in comparison with the corresponding experimental result²⁴ of the doping dependence of the nematic-order state characteristic energy observed from $\text{Bi}_2\text{Sr}_2\text{CaCu}_2\text{O}_{8+\delta}$ in Fig. 3b. The result in Fig. 3a indicates clearly that the magnitude of ω_{\max} is particu-

larly large in the underdoped regime, and then monotonically decreases as the doping concentration is increased, which is fully consistent with the corresponding result obtained experimentally from $\text{Bi}_2\text{Sr}_2\text{CaCu}_2\text{O}_{8+\delta}$. More specifically, in comparison with the experimental results of the doping dependence of the pseudogap energy measured on the same samples of $\text{Bi}_2\text{Sr}_2\text{CaCu}_2\text{O}_{8+\delta}$ ²⁴, this remarkable doping dependence of the nematic-order state characteristic energy in Fig. 3 is also well identical to the corresponding doping dependence of the pseudogap energy over a wide range of doping²⁴. The pseudogap in the framework of the kinetic-energy-driven superconductivity originates from the electron self-energy resulting of the dressing of the electrons due to the electron interaction mediated by a strongly dispersive spin excitation^{36–38}, and then it can be identified as being a region of the electron self-energy effect^{39,40} in which the pseudogap suppresses strongly the electronic density of states for energies $\omega > \bar{\Delta}_{\text{PG}}$, where $\bar{\Delta}_{\text{PG}}$ is the pseudogap energy. The doping dependence of the characteristic energy in theory and experiment is virtually identical to each other and also to the corresponding doping dependence of the pseudogap energy, which therefore is important to confirm the characteristic energy at the C_4 rotation symmetry-breaking can be understood as the natural consequence of the electronic nematic-order state within the pseudogap of cuprate superconductors²⁴.

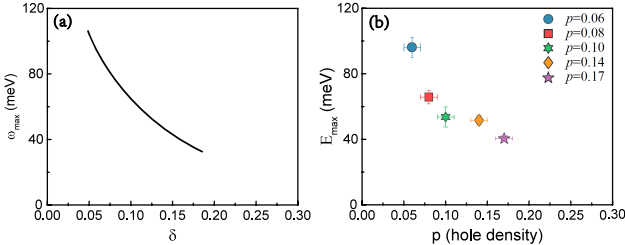


FIG. 3: (Color online) (a) The nematic-order state characteristic energy as a function of doping with $T = 0.002J$ for the strength of the electronic nematicity $\xi = 0.006$. (b) The corresponding experimental result observed from $\text{Bi}_2\text{Sr}_2\text{CaCu}_2\text{O}_{8+\delta}$ taken from Ref. 24.

Now we turn our attention to the possible connection between the nematic-order state characteristic energy and the enhancement of superconductivity. To show this possible connection more clearly, we plot ω_{max} as a function of the strength of the electronic nematicity ξ at $\delta = 0.06$ with $T = 0.002J$ in Fig. 4a. In order to compare the result of the nematic-order state strength dependence of ω_{max} with the corresponding nematic-order state strength dependence of the enhancement of T_c , the corresponding result of T_c as a function of the strength of the electronic nematicity at $\delta = 0.06$ is also shown in Fig. 4b. One can immediately see from the results in Fig. 4 that the strength range together with the *optimal* strength in the nematic-order state strength dependence of ω_{max} is the same with that in the nematic-order state strength dependence of the enhancement of T_c , where

with the increase of the nematic-order state strength, ω_{max} (then T_c) is raised gradually in the weak strength region, and achieves its maximum at around the *optimal* strength $\xi = 0.022$. However, with the further increase of the strength, ω_{max} (then T_c) turns into a monotonically decrease in the strong strength region. This same strength range together with the same *optimal* strength in the nematic-order state strength dependence of the characteristic energy and of the enhancement of SC transition temperature therefore indicates firstly a possible connection between the nematic-order state characteristic energy and the enhancement of superconductivity. On the other hand, it should be also noted that although T_c in Fig. 4b for a given nematic-order state strength at the underdoping $\delta = 0.06$ is much lower than the corresponding T_c at the optimal doping $\delta = 0.15$ obtained in Ref. 25, the global dome-like shape of the nematic-order strength dependence of the enhancement of T_c at the underdoping $\delta = 0.06$ together with the magnitude of the *optimal* strength is the same with that at the optimal doping $\delta = 0.15$, which therefore show that the enhancement of superconductivity caused by the electronic nematicity occurs at any given doping concentration of the SC dome.

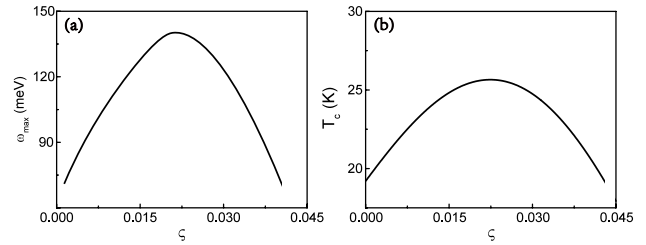


FIG. 4: (Color online) (a) The nematic-order state characteristic energy as a function of the strength of the electronic nematicity ξ with $T = 0.002J$ at $\delta = 0.06$. (b) The corresponding superconducting transition temperature T_c as a function of the strength of the electronic nematicity at $\delta = 0.06$.

In conclusion, within the framework of the kinetic-energy-driven superconductivity, we have studied the doping dependence of the nematic-order state characteristic energy in cuprate superconductors and of its possible connection to the enhancement of superconductivity. Our results show clearly that the nematic-order state characteristic energy is particularly large in the underdoped regime, then it smoothly decreases as the doping concentration is increased, in full agreement with the corresponding to the STS experimental observations. More importantly, our results also indicate firstly that the strength range together with the *optimal* strength in the nematic-order state strength dependence of the characteristic energy is the same with that in the nematic-order state strength dependence of the enhancement of superconductivity. On the basis of these obtained results, the theory therefore predicts a possible connection between the nematic-order state characteristic energy and the enhancement of superconductivity.

Acknowledgements

ZC, XM, and SF are supported by the National Key Research and Development Program of China under Grant No. 2016YFA0300304, and the National Natural

Science Foundation of China (NSFC) under Grant Nos. 11974051 and 11734002. HG is supported by NSFC under Grant Nos. 11774019 and 12074022, and the Fundamental Research Funds for the Central Universities and HPC resources at Beihang University.

* Electronic address: spfeng@bnu.edu.cn

- ¹ J. G. Bednorz and K. A. Müller, *Z. Phys. B* **64**, 189 (1986).
- ² See, e.g., the review, S. L. Cooper and K. E. Grey, in *Physical Properties of High Temperature Superconductors IV*, edited by D. M. Ginsberg (World Scientific, Singapore, 1994), p. 61.
- ³ K. Takenaka, K. Mizuhashi, H. Takagi, and S. Uchida, *Phys. Rev. B* **50**, 6534(R) (1994).
- ⁴ See, e.g., the review, I. M. Vishik, *Rep. Prog. Phys.* **81**, 062501 (2018).
- ⁵ See, e.g., the review, R. Comin and A. Damascelli, *Annu. Rev. Condens. Matter Phys.* **7**, 369 (2016).
- ⁶ See, e.g., the review, Matthias Vojta, *Adv. Phys.* **58**, 699 (2009).
- ⁷ See, e.g., the review, E. Fradkin, S. A. Kivelson, M. J. Lawler, J. P. Eisenstein, and A. P. Mackenzie, *Annu. Rev. Condens. Matter Phys.* **1**, 153 (2010).
- ⁸ See, e.g., the review, R. M. Fernandes, P. P. Orth, and J. Schmalian, *Annu. Rev. Condens. Matter Phys.* **10**, 133 (2019).
- ⁹ S. A. Kivelson and S. Lederer, *Proc. Natl. Acad. Sci.* **116**, 14395 (2019).
- ¹⁰ S. H. Pan, J. P. ÓNeal, R. L. Badzey, C. Chamon, H. Ding, J. R. Engelbrecht, Z. Wang, H. Eisaki, S. Uchida, A. K. Gupta, K.-W. Ng, E. W. Hudson, K. M. Lang, and J. C. Davis, *Nature* **413**, 282 (2001).
- ¹¹ See, e.g., the review, Ø. Fischer, M. Kugler, I. Maggio-Aprile, C. Berthod, and C. Renner, *Rev. Mod. Phys.* **79**, 353 (2007).
- ¹² See, e.g., the review, J.-X. Yin, S. H. Pan, M. Z. Hasan, *Nat. Rev. Phys.* **3**, 249 (2021).
- ¹³ S. Nakata, M. Horio, K. Koshiishi, K. Hagiwara, C. Lin, M. Suzuki, S. Ideta, K. Tanaka, D. Song, Y. Yoshida, H. Eisaki, A. Fujimori, [arXiv:1811.10028](https://arxiv.org/abs/1811.10028).
- ¹⁴ V. Hinkov, D. Haug, B. Fauqué, P. Bourges, Y. Sidis, A. Ivanov, C. Bernhard, C. T. Lin, B. Keimer, *Science* **319**, 597 (2008).
- ¹⁵ Y. Sato, S. Kasahara, H. Murayama, Y. Kasahara, E.-G. Moon, T. Nishizaki, T. Loew, J. Porras, B. Keimer, T. Shibauchi, and Y. Matsuda, *Nat. Phys.* **13**, 1074 (2017).
- ¹⁶ R. Daou, J. Chang, D. LeBoeuf, O. Cyr-Choини́re, F. Laliberté, N. Doiron-Leyraud, B. J. Ramshaw, R. Liang, D. A. Bonn, W. N. Hardy, and L. Taillefer, *Nature* **463**, 519 (2010).
- ¹⁷ O. Cyr-Choини́re, G. Grissonnanche, S. Badoux, J. Day, D. A. Bonn, W. N. Hardy, R. Liang, N. Doiron-Leyraud, and L. Taillefer, *Phys. Rev. B* **92**, 224502 (2015).
- ¹⁸ W. Wang, J. Luo, C. G. Wang, J. Yang, Y. Kodama, R. Zhou, G.-Q. Zheng, *Sci. China-Phys. Mech. Astron.* **64**, 237413 (2021).
- ¹⁹ Y. Ando, K. Segawa, S. Komiya, and A. N. Lavrov, *Phys. Rev. Lett.* **88**, 137005 (2002).
- ²⁰ J. Wu, A. T. Bollinger, X. He, and I. Božović, *Nature* **547**, 432 (2017).
- ²¹ M. J. Lawler, K. Fujita, J. Lee, A. R. Schmidt, Y. Kohsaka, C. K. Kim, H. Eisaki, S. Uchida, J. C. Davis, J. P. Sethna, and E.-A. Kim, *Nature* **466**, 347 (2010).
- ²² K. Fujita, C. K. Kim, I. Lee, J. Lee, M. H. Hamidian, I. A. Firsov, S. Mukhopadhyay, H. Eisaki, S. Uchida, M. J. Lawler, E.-A. Kim, J. C. Davis, *Science* **344**, 612 (2014).
- ²³ Y. Zheng, Y. Fei, K. Bu, W. Zhang, Y. Ding, X. J. Zhou, J. E. Hoffman, and Y. Yin, *Sci. Rep.* **7**, 8059 (2017).
- ²⁴ S. Mukhopadhyay, R. Sharma, C. K. Kim, S. D. Edkins, M. H. Hamidian, H. Eisaki, S. Uchida, E.-A. Kim, M. J. Lawler, A. P. Mackenzie, J. C. S. Davis, and K. Fujita, *Proc. Natl. Acad. Sci.* **116**, 13249 (2019).
- ²⁵ Z. Cao, Y. Liu, H. Guo, and S. Feng, [arXiv:2105.14494](https://arxiv.org/abs/2105.14494).
- ²⁶ Q.-H. Wang and D.-H. Lee, *Phys. Rev. B* **67**, 020511 (2003).
- ²⁷ D. Gao, Y. Mou, Y. Liu, S. Tan, and S. Feng, *Phil. Mag.* **99**, 752 (2019).
- ²⁸ U. Chatterjee, M. Shi, A. Kaminski, A. Kanigel, H. M. Fretwell, K. Terashima, T. Takahashi, S. Rosenkranz, Z. Z. Li, H. Raffy, A. Santander-Syro, K. Kadowaki, M. R. Norman, M. Randeria, and J. C. Campuzano, *Phys. Rev. Lett.* **96**, 107006 (2006).
- ²⁹ Y. He, Y. Yin, M. Zech, A. Soumyanarayanan, M. M. Yee, T. Williams, M. C. Boyer, K. Chatterjee, W. D. Wise, I. Zeljkovic, T. Kondo, T. Takeuchi, H. Ikuta, P. Mistark, R. S. Markiewicz, A. Bansil, S. Sachdev, E. W. Hudson, J. E. Hoffman, *Science* **344**, 608 (2014).
- ³⁰ P. W. Anderson, *Science* **235**, 1196 (1987).
- ³¹ Ying-Jer Kao and Hae-Young Kee, *Phys. Rev. B* **72**, 024502 (2005).
- ³² B. Edegger, V. N. Muthukumar, and C. Gros, *Phys. Rev. B* **74**, 165109 (2006).
- ³³ A. Wollny and M. Vojta, *Physica B* **404**, 3079 (2009).
- ³⁴ K. Lee, S. A. Kivelson, and E.-A. Kim, *Phys. Rev. B* **94**, 014204 (2016).
- ³⁵ S. Feng, *Phys. Rev. B* **68**, 184501 (2003); S. Feng, T. Ma, and H. Guo, *Physica C* **436**, 14 (2006).
- ³⁶ S. Feng, H. Zhao, and Z. Huang, *Phys. Rev. B* **85**, 054509 (2012); *Phys. Rev. B* **85**, 099902(E) (2012).
- ³⁷ See, e.g., the review, S. Feng, Y. Lan, H. Zhao, L. Kuang, L. Qin, and X. Ma, *Int. J. Mod. Phys. B* **29**, 1530009 (2015).
- ³⁸ S. Feng, L. Kuang, and H. Zhao, *Physica C* **517**, 5 (2015).
- ³⁹ See, e.g., the review, T. Timusk and B. Statt, *Rep. Prog. Phys.* **62**, 61 (1999).
- ⁴⁰ See, e.g., the review, S. Hüfner, M. A. Hossain, A. Damascelli, and G. A. Sawatzky, *Rep. Prog. Phys.* **71**, 062501 (2008).